Appl. Phys. A 88, 49–56 (2007)
DOI: 10.1007/s00339-007-3975-z

Applied Physics A
Materials Science & Processing

D.J. ROGERS[1,2,✉]
F. HOSSEINI TEHERANI[1]
A. LARGETEAU[3]
G. DEMAZEAU[3]
C. MOISSON[4]
D. TUROVER[4]
J. NAUSE[5]
G. GARRY[6]
R. KLING[7]
T. GRUBER[7]
A. WAAG[8]
F. JOMARD[9]
P. GALTIER[9]
A. LUSSON[9]
T. MONTEIRO[10]
M.J. SOARES[10]
A. NEVES[10]
M.C. CARMO[10]
M. PERES[10]
G. LERONDEL[2]
C. HUBERT[2]

ZnO homoepitaxy on the O polar face of hydrothermal and melt-grown substrates by pulsed laser deposition

[1] Nanovation SARL, 103bis, rue de Versailles, 91400 Orsay, France
[2] Technical University of Troyes-CNRS (FRE2671), 12 rue Marie Curie, BP 2060, 10010 Troyes, France
[3] ICMCB-CNRS, Bordeaux 1 University (Science & Technology), 87 Av. A. Schweitzer, 33608 Pessac, France
[4] Novasic, Savoie Technolac, Arche Bât. 4, BP 267, 73375 Le Bourget du Lac, France
[5] Cermet Inc., 1019 Collier Road, Atlanta, GA 30318, USA
[6] Thales Research, Domaine de Corbeville, 91401 Orsay, France
[7] Department of Semiconductor Physics, Ulm University, 89069 Ulm, Germany
[8] Institute of Semiconductor Technology, Braunschweig Technical University, 38106 Braunschweig, Germany
[9] LPSC-CNRS, 1 Place Aristide Briand, 92195 Meudon, France
[10] Physics Department, University of Aveiro, 3810-193 Aveiro, Portugal

Received: 9 December 2005/Accepted: 13 January 2007
Published online: 18 April 2007 • **© Springer-Verlag 2007**

ABSTRACT 2 cm diameter hydrothermal ZnO crystals were grown and then made into substrates using both mechanical and chemical-mechanical polishing (CMP). CMP polishing showed superior results with an (0002) Ω scan full width half maximum (FWHM) of 67 arcsec and an root mean square (RMS) roughness of 2 Å. In comparison, commercial melt-grown substrates exhibited broader X-ray diffraction (XRD) linewidths with evidence of sub-surface crystal damage due to polishing, including a downward shift of *c*-lattice parameter. Secondary ion mass spectroscopy revealed strong Li, Fe, Co, Al and Si contamination in the hydrothermal crystals as opposed to the melt-grown substrates, for which glow discharge mass spectroscopy studies had reported high levels of Pb, Fe, Cd and Si. Low temperature photoluminescence (PL) studies indicated that the hydrothermal crystal had high defect and/or impurity concentrations compared with the melt-grown substrate. The dominant bound exciton for the melt-grown substrate was indexed to Al. ZnO films were grown using pulsed laser deposition. The melt-grown substrates gave superior results with XRD (0002) Ω and $2\theta/\Omega$ WHM of 124 and 34 arcsec, respectively. Atomic force microscope measurements indicated a low RMS roughness (1.9 nm) as confirmed by fringes in the XRD $2\theta/\Omega$ scan. It was suggested that the improvement in XRD response relative to the substrate might be due to "healing" of sub-surface polishing damage due to the elevated T_s used for the growth. Indeed the *c*-lattice parameter for the homoepitaxial layer on the melt-grown substrate had become that which would be expected for strain-free ZnO. Furthermore, the stability of the PL peak positions relative to bulk ZnO, confirmed that the films appear practically strain free.

PACS 81.10.h; 68.55.-a; 81.15.Fg; 78.20.-e; 61.82.Fk; 61.10.Nz; 68.37.Ps

✉ Fax: +33 1 64 46 29 49, E-mail: DRogers610@aol.com

1 Introduction

Wurtzite ZnO has long been known as a remarkable multi-functional material with a very distinctive set of intrinsic properties including: a wide bandgap (~ 3.37 eV) [1], a large exciton binding energy (~ 60 meV) [2], a high melting point (2248 K), a high radiation resistance [3], a very high shear modulus (~ 45.5 GPa), high transparency in the visible spectrum [4], one of the highest piezoelectric coefficients of all semiconductors [5], an amenability to wet chemical etching, low toxicity and low material costs. As a result, there is already a whole range of established applications based on ZnO including, piezoelectric transducers, gas sensors, surface acoustic wave devices, transparent conducting oxides and varistors [4, 6, 7].

Recently, there has been a surge in the research on ZnO. This is linked to a number of discoveries plus advances in the capacity to engineer the extrinsic properties of ZnO. These include demonstrations of high quality epitaxy [8–11], low threshold room temperature (RT) laser action [12, 13], stimulated excitonic emission up to 550 K [1, 14], p-type doping [15–19], band gap engineering from 2.8 to 4 eV [20], Schottky and ohmic contacts [21], self-forming laser cavities [22] and a propensity for generation of a phenomenally wide range of nanostructures [23]. ZnO has also been identified as a prime candidate for RT ferromagnetism in a semiconductor material [24, 25]. This rapid evolution heralds the emergence of ZnO in many novel applications, including ultraviolet (UV) light emission/detection [26], high power transparent electronics [27], spintronics [25] and nanotechnology [23].

Interestingly, the vast majority of the recent work on ZnO has been conducted on ZnO films grown on sapphire substrates (corundum structure) [8–11]. Sapphire is chosen in

spite of considerable lattice and thermal mismatches between the two materials. In theory, single crystal ZnO would present a much better platform for ZnO film growth. This is because ZnO substrates have no lattice or thermal mismatch with ZnO epilayers, so we can expect simplified epitaxy, strain free layers with much reduced defect density and the possibility to control film polarity via choice of substrate surface polarity (O-face or Zn face). In addition, the fabrication of devices can be simplified, compared to ZnO on sapphire, because ZnO substrates can be made conducting and are amenable to chemical etching.

In spite of the wide availability of ZnO substrates, however, reports of ZnO homoepitaxy are scarce [28–33] and high quality homoepitaxy has proven more difficult than expected. This has been attributed to a number of factors, including

1. a highly variable quality of substrate crystal structure and purity [34] (a large proportion of commercial ZnO substrates turn out to be polycrystalline),
2. a variable quality of polishing, which has been shown to have a dramatic impact on the crystal structure and surface [35],
3. considerable differences between the required growth conditions and obtained layer qualities for the different polar surfaces of the ZnO substrate [28–33],
4. the observation that the elevated substrate temperatures (T_s) commonly used for ZnO epitaxy can provoke a degradation of the substrate surface morphology and crystal quality [36, 37],
5. a hydroxide layer at the ZnO surface which may complicate the epitaxy [38],
6. a cost-level for device-grade ZnO substrates which is almost two orders of magnitude higher than for *c*-sapphire.

Although this last factor is not technical, it has hampered the adoption of ZnO substrates by the research community as a whole and thus limited the kind of systematic studies necessary to establish procedures for high quality homoepitaxy.

In this work, we examine these issues by studying how to obtain high quality ZnO substrates and high quality homoepitaxy. In order to do this, we developed hydrothermal ZnO substrates and compared their quality with that of commercial, melt-grown ZnO substrates. We then performed pulsed laser deposition (PLD) growth of ZnO films on the O polar face of both types of substrate. Compared to other growth techniques, PLD has the advantage of significantly higher adatom mobility at lower T_s [39]. Hence, high quality epitaxy should be possible at lower T_s than is feasible with other growth techniques and the potentially negative impact of elevated T_s on the substrate surface can be reduced.

2 Experiment

2.1 *Bulk crystal growth*

ZnO hydrothermal crystals were grown using the experimental set-up shown in Fig. 1. In this approach ZnO ceramic nutrients (at the bottom of the autoclave) are dissolved in an alkaline solution held at high pressure. A small temperature gradient provokes a circulation of the solution through the diaphragm and the lower temperature at the top of the autoclave induces a condensation of ZnO on seeds suspended on a platinum wire. For crystals in this study the duration of growth was 2 weeks.

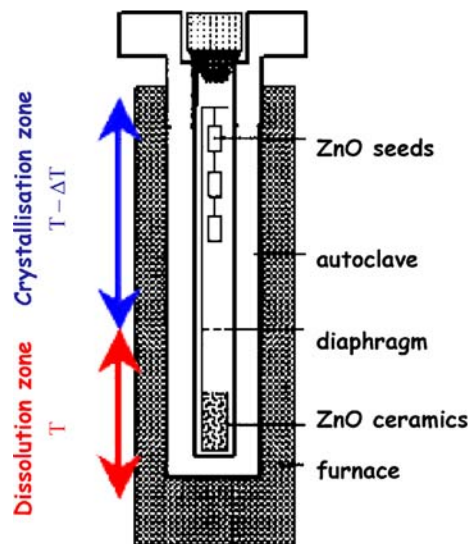

FIGURE 1 Schematic diagram of autoclave used for hydrothermal growth of ZnO crystals

2.2 *Substrate preparation*

The hydrothermal crystals were diced using a diamond saw and then polished. Two different polishing techniques (mechanical polishing (MP) and chemical mechanical polishing (CMP)) were employed for sake of comparison. The MP was a standard approach employing abrasion with progressively finer diamond powder solutions followed by a final buffing stage with a fine-grain cloth so as to obtain a mirror-like surface. The CMP was a proprietary (Novasic) approach, specifically designed for ZnO, so as to minimize both surface roughness and sub-surface damage.

"Production grade" commercial Bridgman (melt-grown) substrates were provided by Cermet Inc. Their preparation conditions are described elsewhere [40, 41].

2.3 *Pulsed laser deposition*

ZnO films were grown by PLD of a sintered ZnO powder target with a 248 nm KrF excimer laser. The O polar face was chosen because it has been found to be more stable at elevated T_s [36] and because layers grown on the O polar face are reported to show better quality epitaxy [42, 43]. There was no pre-growth preparation of the substrate surface by chemical cleaning or annealing because this has been shown to strongly influence the quality of the subsequent epitaxial layer [38, 44]. A single step growth at 500 °C was performed under 5×10^{-4} Torr of oxygen with a laser frequency of 5 Hz and a substrate-to-target distance of 4 cm.

2.4 *Characterization*

Crystal structure was studied using a high resolution X-ray diffraction (XRD) system. The spot size at the sample was $\sim 5\ \text{mm} \times 5\ \text{mm}$. Surface morphology was investigated using a Park Scientific Instruments M5 nanoprobe atomic force microscope (AFM) in contact-mode. Qualitative

measurement of chemical composition was performed using secondary ion mass spectroscopy (SIMS). Optical properties were studied using above and below bandgap, low temperature photoluminescence (PL) with a 325 nm HeCd laser and several lines of an Ar^+ laser. Raman spectroscopy was performed at RT in backscattering geometry using the 514.5 nm line of an Ar^+ laser.

Resistivity was measured using a 4 point pressure contact system.

3 Results and discussion

3.1 *Hydrothermal crystal*

The highest quality crystals were obtained using a KOH (3 M) + LiOH (1 M) solvent with a temperature (T) of 360 °C, a temperature drop (ΔT) of 10 °C and a pressure of 150 MPa.

Figure 2 shows an image of the hydrothermal crystal after growth with a mm grid in the background to illustrate the scale. The crystal is about 2 cm in diameter. The top part of the crystal in the cross-sectional image is dark green in color while the bottom part is paler. Such orientation-dependent coloration is typical of hydrothermal ZnO and has been linked to enhanced incorporation of impurities at the slower-growing O-face during the growth [45, 46]. This allowed us to identify the top surface in the cross-sectional image as the O-face.

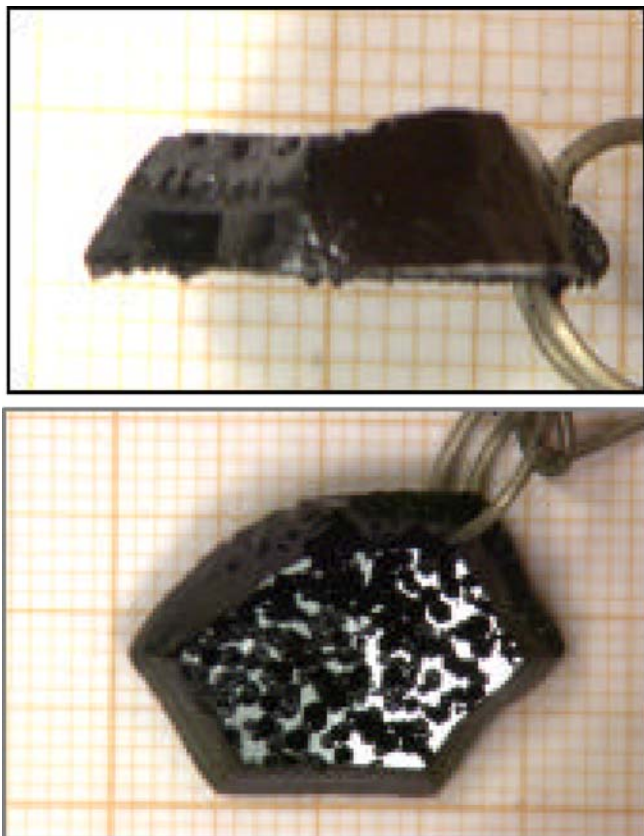

FIGURE 2 Image of raw ZnO hydrothermal crystal. In the image we can see a cross-sectional view in which the seed crystal (*below*) and the hydrothermal growth (*above*) can be discriminated. In the *lower* image we can see a top view of the growth surface

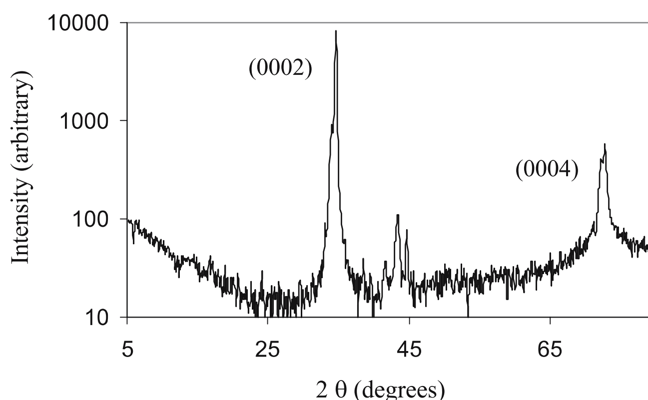

FIGURE 3 X-ray diffraction 2θ–Ω scan for the hydrothermal ZnO crystal

Substrate	Contaminant	Concentration
Hydrothermal (SIMS)	Li, Fe, Co, Al, Si	Significant
	Mn, Mg	Moderate
	C	Little
Melt grown (GDMS)	Pb	8 ppm
	Fe	4 ppm
	Cd	2.5 ppm
	Si	1.4 ppm
	Cl	0.9 ppm
	S	0.8 ppm
	Al	0.6 ppm

TABLE 1 SIMS and GDMS data for the hydrothermal and melt-grown substrates

Figure 3 shows the XRD 2θ–Ω scan for the O-face growth surface. The strong narrow peaks, and their 2θ angular positions, are characteristic of ZnO with preferred (0002) orientation.

Table 1 compares the results of SIMS of the hydrothermal crystal with glow discharge mass spectroscopy (GDMS) data reported for a typical Cermet melt-grown substrate [47]. The hydrothermal crystal shows strong contamination with Li, Fe, Co, Al and Cu. The Li probably comes from the LiOH in the solvent. Li is a fast diffuser and can act as an acceptor in ZnO. It is not desirable because it can readily diffuse from the substrate into the film and modify the electrical properties. Unfortunately, LiOH is required in the solvent because Li slows the growth and improves crystal quality, stoichiometry and surface morphology [48]. The Fe signal probably comes partly from the walls of the autoclave since KOH also dissolves the autoclave itself. This can be prevented by use of a Pt liner. The melt-grown substrate shows strong contamination with Pb, Fe, Cd and Si. It is interesting to note that Li does not figure in the contaminants detected for the melt-grown substrate.

3.2 *Substrate evaluation*

Typical (0002) peak XRD spectra and AFM images of the substrates are shown in Figs. 4 and 5, respectively. Table 2 summarizes the main features. The full width half maximum (FWHM) of the XRD 2θ–Ω scans are similar for all the substrates (between 180 and 187 arcsec). Close inspection of the peak shapes reveals that they are not perfectly symmetrical. This signifies several strongly aligned crystallo-

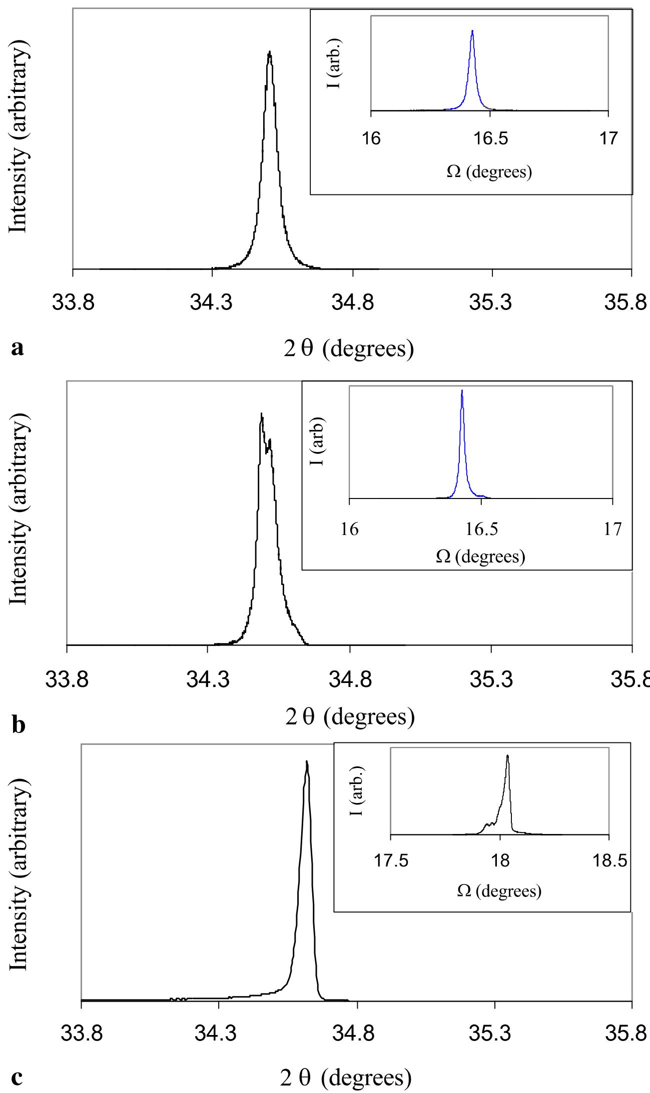

FIGURE 4 2θ–Ω and Ω XRD scans for (0002) peak of (**a**) MP hydrothermal substrate (**b**) CMP hydrothermal substrate (**c**) melt-grown substrate

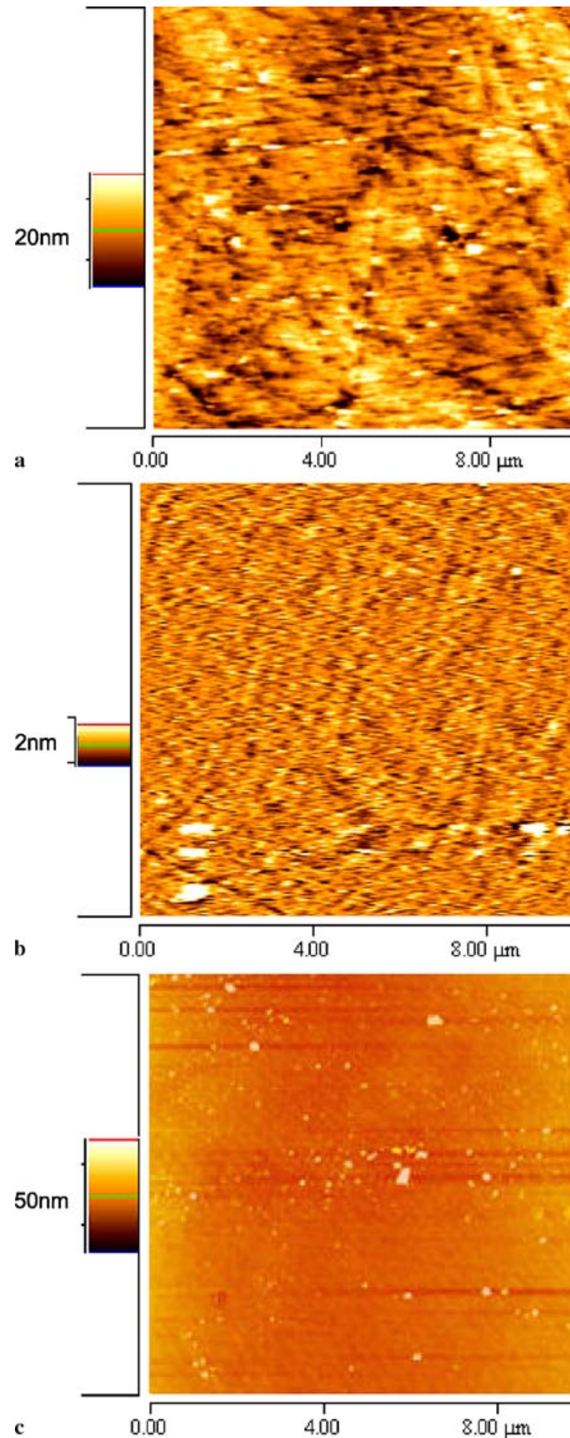

FIGURE 5 Contact mode AFM images for (**a**) MP hydrothermal substrate (**b**) CMP hydrothermal substrate (**c**) melt-grown substrate. The roughness for these samples is near the detection limit for the AFM so the absolute values for RMS roughness may not necessarily be correct. The differences in roughness between the samples were very reproducible, however

graphic domains rather than a coherent single crystal. For the melt-grown sample, there is also a pronounced tail on the peak at lower 2θ angles. Other studies have linked such an effect to sub-surface damage induced by the polishing [35] (N.B. this kind of XRD study is only sensitive to the first few microns at the sample surface). The c lattice parameter for the hydrothermal substrates is typical for ZnO, but that for the melt-grown substrate is smaller than expected. This suggests that the crystal is under compressive strain, which is consistent with a damaged sub-surface layer due to the polishing.

The inset Ω-scan spectra reveal significant differences between the three samples. The FWHM for the CMP hydrothermal, at 67 arcsec, is significantly smaller than that for the MP hydrothermal: 107 arcsec (N.B. smaller Ω-scan FWHM is indicative of reduced dispersion of the crystal orientation). This suggests that CMP produces less sub-surface damage. The Ω-scan FWHM for the melt-grown substrate, at 223 arcsec, is larger again. Since there is no comparative data on the polishing, however, it is not clear whether this reflects the polishing or the underlying crystal quality.

AFM study revealed RMS roughnesses of 0.2, 0.9 and 2.2 nm, respectively, for the CMP hydrothermal, melt-grown and MP hydrothermal. The absolute roughness values are not necessarily exact because they are close to the detection limit for the AFM. The relative roughnesses are quite reproducible, however. AFM also revealed evidence of particles on the substrate for the MP hydrothermal and melt-grown substrates.

TABLE 2 SIMS XRD and AFM data for the ZnO substrates

	Crystal	c lattice parameter (Å)	$2\theta/\Omega$ scan FWHM (arcsec)	Ω scan FWHM (arcsec)	RMS roughness (nm)	Peak/valley roughness (nm)
ZnO substrate	Hydrothermal (MP)	5.21	180	109	2.2	38
	Hydrothermal (CMP)	5.21	180	67	0.2	1
	Melt-grown	5.18	187	223	0.9	33

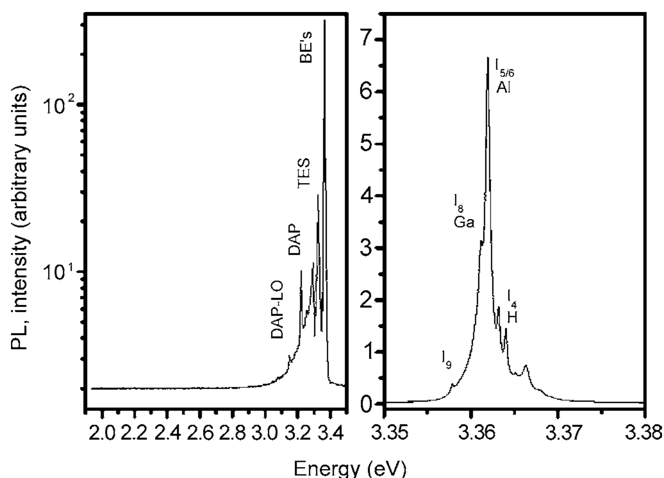

FIGURE 6 10 K PL spectrum for melt-grown ZnO substrate obtained with above band gap excitation. Please pay attention to the differences between the scales used in the respective plots

These particles may be left-over debris from the polishing. The CMP hydrothermal substrate appears to have far fewer of these particles.

No significant PL signal was observed for the hydrothermal crystal. This could be due to non-radiative recombination centers in the crystal (e.g., impurities or defects) or problems with surface reflection. Figure 6 shows the 10 K PL spectrum for the melt-grown substrate. There is negligibly low green emission, which has been linked to low intrinsic defect density (particularly neutral oxygen vacancies [49]) and/or low impurity concentration (often linked to Cu [50]). The luminescence is dominated by higher energy transitions related to bound exciton recombination (BE's), its two-electron-satellites (TES) and the 3.22 eV donor acceptor pair recombination (DAP). Assignments of the bound exciton recombinations were made by comparison with literature [51]. Interestingly, the dominant bound exciton seems to be related to Al rather than hydrogen. This is consistent with a relatively low hydrogen concentration in the melt-grown substrate.

Figure 7 shows the RT Raman spectra for the hydrothermal crystal and melt-grown substrate. The spectra are similar and are indicative of low strain and high crystal quality for both.

The electrical resistivities measured for the O-faces of the hydrothermal and melt grown substrates were ~ 200 kΩ cm and ~ 1 kΩ cm, respectively. The hydrothermal crystal showed more variations across the crystal while the melt-grown substrate had a relatively homogeneous resistivity.

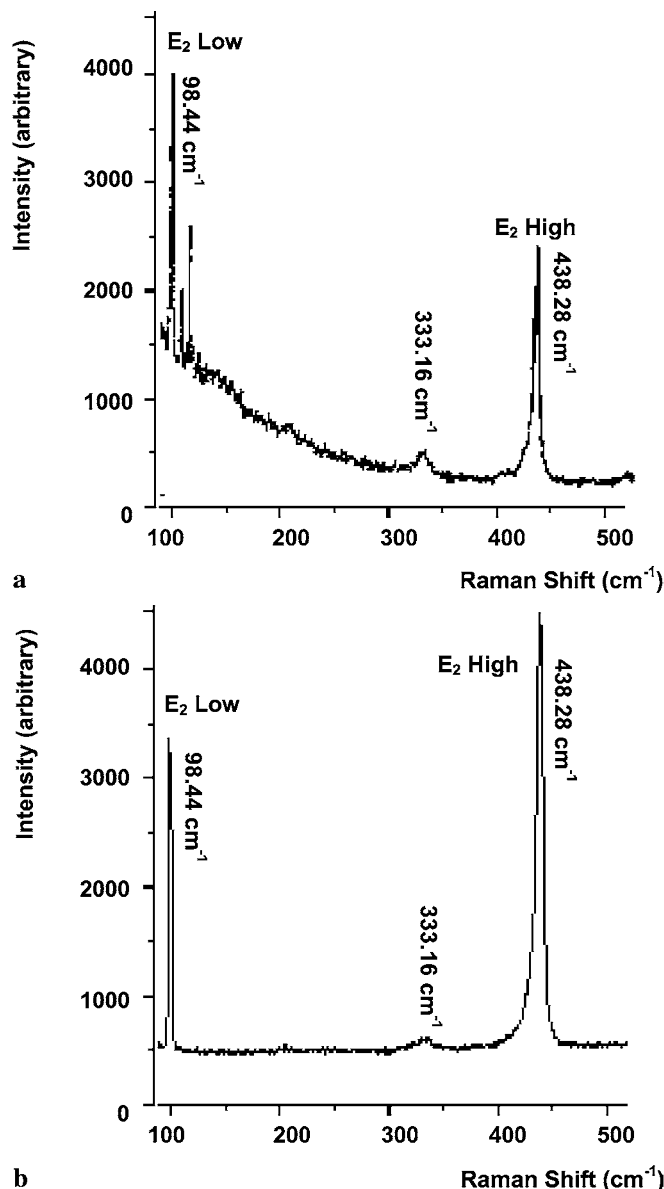

FIGURE 7 RT Raman spectra for (**a**) hydrothermal and (**b**) melt-grown substrates (N.B. the differences in the background signal are linked to different measurement configurations rather than differences between the samples)

3.3 *Homoepitaxy*

Typical (0002) peak XRD spectra and AFM images for the homoepitaxial samples on the CMP hydrothermal and the melt-grown substrates are shown in Figs. 8, 9 and 10. Table 3 summarizes the main features of the XRD and AFM analysis.

The Ω-scan FWHM for the CMP hydrothermal substrate is 173 arcsec. This is more than twice as wide as for the substrate prior to growth (67 arcsec). Hence, we were not able to replicate the low crystallographic dispersion of substrate crystal quality in the epilayer. This is not the case for the melt-grown substrate, however. The Ω-scan FWHM (at 124 arcsec)

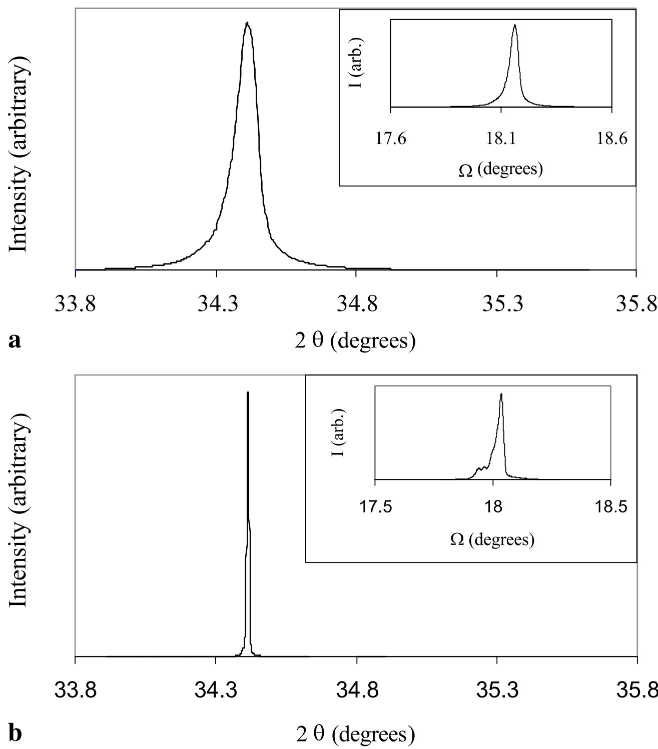

FIGURE 8 2θ–Ω and Ω XRD scans for (0002) peak of homoepitaxial film on (**a**) CMP hydrothermal substrate (**b**) melt-grown substrate

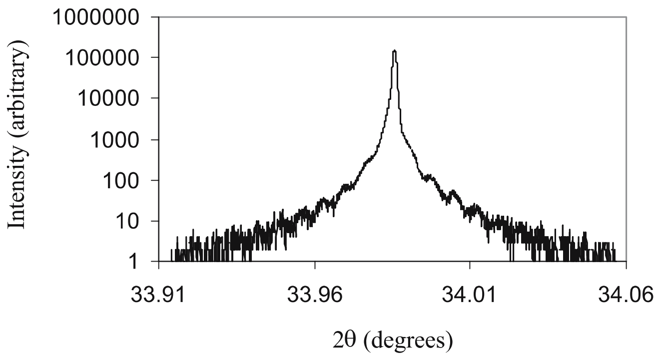

FIGURE 9 Log scale blow-up of 2θ–Ω XRD scan for the (0002) peak of homoepitaxial film on melt-grown substrate

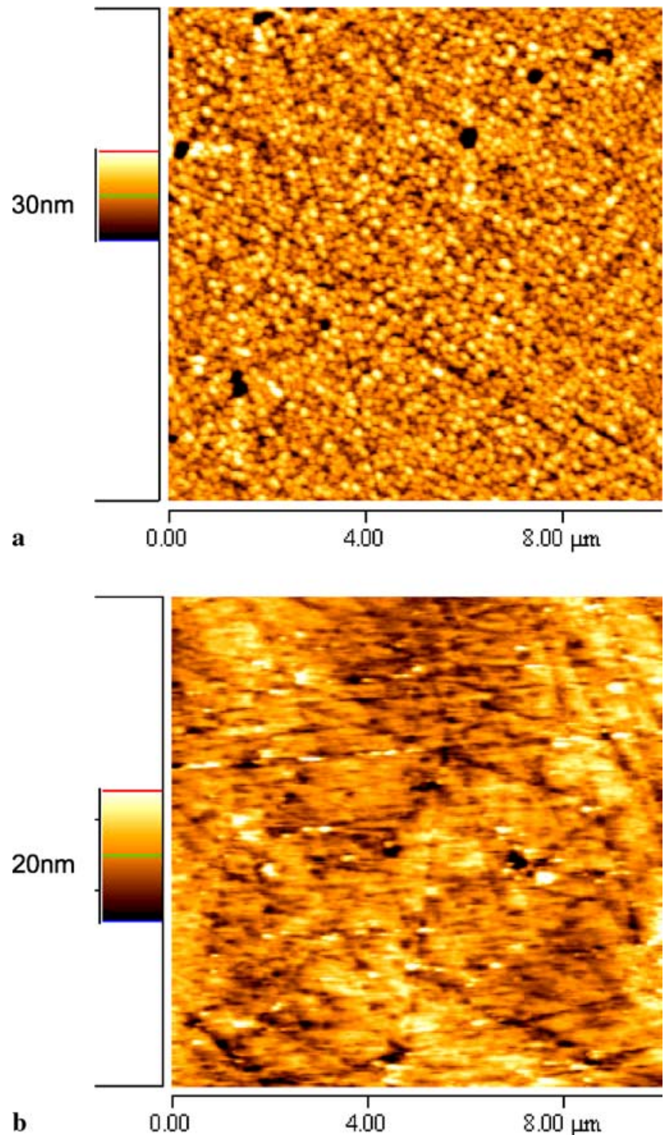

FIGURE 10 Contact mode AFM images for homoepitaxial film on (**a**) CMP hydrothermal substrate (**b**) melt-grown substrate

is better than for the homoepitaxy on the hydrothermal substrate and even shows an improvement compared to the value of 223 arcsec prior to growth.

The XRD 2θ–Ω scan for the CMP hydrothermal substrate is about twice as large as for the substrate without the epitaxial layer. The melt-grown substrate, on the other hand, shows a dramatically reduced FWHM, of 34 arcsec, compared with the substrate prior to growth (228 arcsec). The origin of this marked improvement in crystal quality is not clear but it has been suggested that elevated T_s can provoke surface recrystallisation ,which "heals" the polish damage in the sub-surface layer [31]. Indeed, there is no longer a tail, at lower 2θ angle, on the peak for the melt-grown sample. Careful inspection, Fig. 9, reveals periodic oscillations in the skirt of the peak originating from interference between reflections from the substrate/layer interface and the film surface. Their presence indicates that the film has excellent surface morphology with low roughness over a wide area. The fringe spacing gives an estimate of the film thickness at about 170 nm, which corresponds to a film growth rate of about 5.7 Å per minute. This is comparable to the rate for control samples grown under simi-

	Crystal	c lattice parameter (Å)	$2\theta/\Omega$ scan FWHM (arcsec)	Ω scan FWHM (arcsec)	RMS roughness (nm)	Peak/valley roughness (nm)
ZnO homoepitaxy	Hydrothermal (CMP)	5.21	334	173	5.4	96
	Melt-grown	5.21	34	124	1.9	50

TABLE 3 XRD and AFM results for the homoepitaxial films

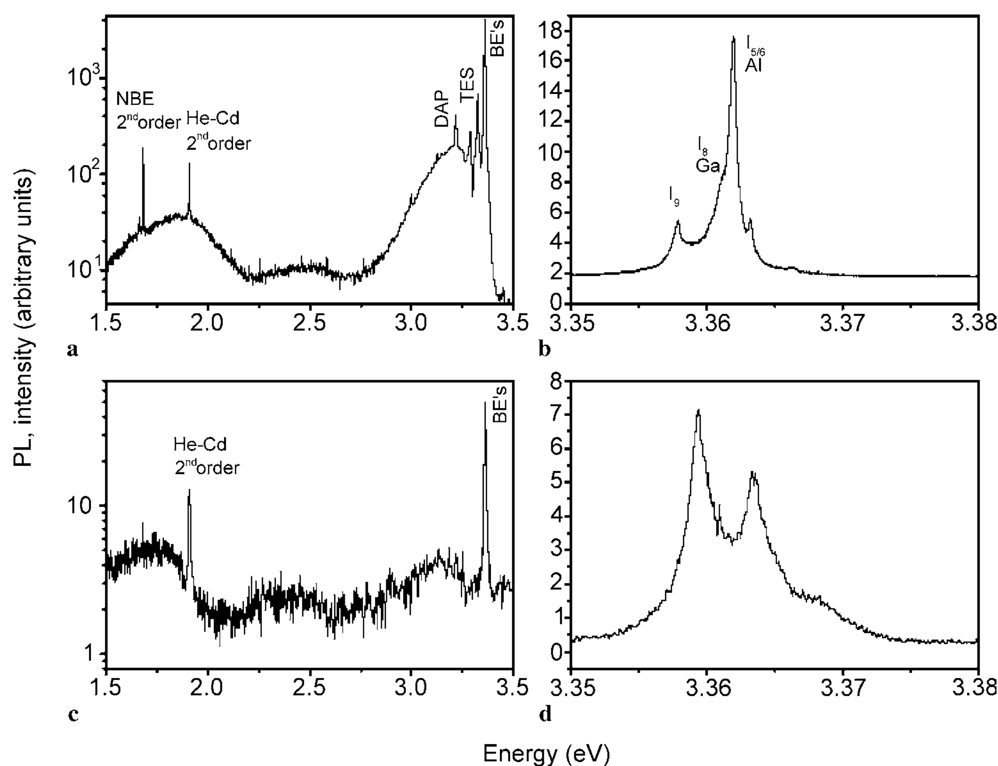

FIGURE 11 10 K PL spectra for homoepitaxial films obtained with above band gap excitation: (**a**) and (**b**) grown on melt-grown substrate and (**c**) and (**d**) on the CMP hydrothermal substrate. Please pay attention to the differences between the scales used in the respective plots

lar conditions on c-sapphire. At 5.21 Å, the c lattice parameter for both the films is typical for relaxed ZnO.

The excellent surface morphology of the homoepitaxial layer on the melt-grown substrate was confirmed by AFM study which gave an RMS roughness of ~ 1.9 nm over $10\ \mu m \times 10\ \mu m$. This is significantly lower than the roughness measured for the homoepitaxy on the hydrothermal substrate (N.B. AFM of the CMP hydrothermal substrate prior to growth (Table 2) revealed a lower roughness than for the melt-grown substrate).

Resistivity could not be estimated accurately for the film using the four-point method because the conducting nature of the substrates meant that there was no current confinement in the homoepitaxial layer.

Figure 11 shows the ~ 10 K PL spectra observed for the homoepitaxial samples. The spectrum for the film grown on the melt-grown substrate (a) shows quite narrow BE lines compared with those observed for the film on the CMP hydrothermal substrate (b). Furthermore, comparing Figs. 11 and 6 reveals that there is no shift in the BE peak position. This suggests that the homoepitaxial layers have no appreciable strain. The I4-H related bound exciton is seen to be lower (or even disappear) in the film compared to the substrate. New optical centres are developed, as evidenced by the appearance of a broad UV band and an orange/red luminescence (peaked at 3.0 eV and 1.8 eV, respectively). The same UV band and orange/red emission are present for the film grown on the CMP hydrothermal substrate.

4 Conclusion

2 cm diameter ZnO crystals were produced using hydrothermal growth and then made into substrates by both MP and CMP. XRD and AFM studies indicated excellent crystal quality and surface morphology for the CMP substrate (Ω-scan FWHM of 67 arcsec and RMS roughness < 1 nm). These characteristics compared very favorably with those of commercial melt-grown substrates, which showed indications of sub-surface polishing damage (broadened peaks, downward shift in c lattice parameter and the appearance of an extended tail on the lower angle side of the (0002) peak in 2θ–Ω scans). SIMS showed strong Li, Fe, Co, Al and Si contamination in the hydrothermal crystals as opposed to the melt-grown substrates, for which GDMS studies [47] reported high levels of Pb, Fe, Cd and Si. Low temperature PL studies indicated that the hydrothermal crystal had relatively high defect and/or impurity levels as opposed to the melt-grown substrate, which showed a very low defect/impurity related signal. The dominant bound exciton for the melt-grown substrate was indexed to Al rather than H, which correlated well with the SIMS results.

PLD growth of ZnO on the CMP hydrothermal substrate failed to match the crystal quality or surface morphology of the substrate. PLD growth on the melt-grown substrate, however, gave excellent crystal quality films with even better XRD results than for the substrate (a Ω-scan (0002) peak FWHM of 124 arcsec and a $2\theta/\Omega$ scan with a FWHM of 34 arcsec). In addition, AFM measurements indicated a very low RMS roughness (over $10\ \mu m \times 10\ \mu m$) of 1.9 nm as confirmed by the appearance of fringes in the skirt of the (0002) peak XRD $2\theta/\Omega$ scan. It was suggested that the improvement in XRD response relative to the substrate alone might be due to healing of the sub-surface polishing damage due to the elevated T_s used for the growth. Indeed the c-lattice parameter for the homoepitaxial layer on the melt-grown substrate had become that which would be expected for strain-free ZnO. Furthermore, the stability of the peak positions observed in

PL studies, relative to relaxed bulk ZnO, confirmed that the films appear practically strain free. PL studies also revealed the appearance of new optical centers in the homoepitaxial layers.

ACKNOWLEDGEMENTS The authors would like to thank R. Triboulet, M. Kawasaki, B. Nemeth, C. Litton and M. Callahan for useful discussions. This study is the result of a collaboration between a large number of European research groups and companies with wide-ranging and complementary competences. We would like to thank the European Commission for initiating and facilitating this collaboration through funding of the ZnO-focused SOXESS (semiconductor oxides for UV opto electronics, surface acoustics and spintronics) thematic network. One of the authors (Nanovation) would also like to thank the French Ministry of Research, l'Agence Nationale Pour la Valorisation de la Recherche, CRITT, Scientipole, the incubator Incuballiance, l'Institut d'Electronique Fondamental at Orsay University, Varian, Coherent, Messer and CLT Mecanique for support in this work. M. Peres, would like to thank Fundação para a Ciência e Tecnologia (Portugal) for his grant. This work was partially funded by FCT/FEDER (POCTI/CTM/45236/02) and FCT/FEDER (POCTI/FAT/48822/02).

REFERENCES

1 D.M. Bagnall, Y.F. Chen, Z. Zhu, T. Yao, M.Y. Shen, T. Goto, Appl. Phys. Lett. **73**, 1038 (1998)
2 P. Zu, Z.K. Tang, G.K.L. Wong, M. Kawasaki, A. Ohtomo, H. Koinuma, Y. Segawa, Solid State Commun. **103**, 459 (1997)
3 D.C. Look, Mater. Sci. Eng. B **80**, 383 (2001)
4 R.G. Gordon, MRS Bull. **25**, 8 (2000)
5 T. Sciosaki, N. Kitamura, A. Kawabata, Proc. IEEE Ultrasonics Symp. 296 (1991)
6 Y.P. Wang, W.I. Lee, T.Y. Tseng, Appl. Phys. Lett. **69**, 1807 (1996)
7 R. Triboulet, Proc. SPIE **4412**, 1 (2001)
8 Y. Chen, D.M. Bagnall, H.J. Ko, K. Park, K. Hiraga, Z. Zhu, T. Yao, J. Appl. Phys. **84**, 3912 (1998)
9 P. Fons, K. Iwata, S. Niki, A. Yamada, K. Matsubara, J. Cryst. Growth **201**–**202**, 627 (1999)
10 K. Sakurai, M. Kanehiro, K. Nakahara, T. Tanabe, S. Fujita, S. Fujita, J. Cryst. Growth **209**, 522 (2000)
11 T. Onishi, A. Ohtomo, M. Kawasaki, K. Takahashi, M. Yoshimoto, H. Koinuma, Appl. Phys. Lett. **72**, 824 (1998)
12 D.C. Reynolds, D.C. Look, B. Jogai, Solid State Commun. **103**, 459 (1996)
13 D.M. Bagnall, Y.F. Chen, Z. Zhu, T. Yao, S. Koyama, M.Y. Shen, T. Goto, Appl. Phys. Lett. **70**, 2230 (1997)
14 Z.K. Tang, G.K.L. Wong, P. Yu, M. Kawasaki, A. Ohmoto, H. Koinuma, Y. Segawa, Appl. Phys. Lett. **72**, 3270 (1998)
15 K. Mengishi, Y. Kowai, Y. Kikuchi, K. Yano, M. Kasuga, A. Shimizu, Japan. J. Appl. Phys. **36**, L1453 (1997)
16 M. Joseph, H. Tabata, T. Kawai, Japan. J. Appl. Phys. **38**, L1205 (1999)
17 Y.R. Ryu, S. Zhu, D.C. Look, J.M. Wrobel, H.M. Jeong, H.W. White, J. Cryst. Growth **216**, 330 (2000)
18 D.C. Look, D.C. Reynolds, C.W. Litton, R.L. Jones, D.B. Eason, G. Cantwell, Appl. Phys. Lett. **81**, 1830 (2002)
19 K.-K. Kim, H.-S. Kim, D.-K. Hwang, J.-H. Lim, S.-J. Park, Appl. Phys. Lett. **83**, 63 (2003)
20 A. Ohtomo, M. Kawasaki, T. Koida, M. Masubuschi, H. Koinuma, Y. Sakurai, Y. Yoshida, T. Yasuda, Y. Segawa, Appl. Phys. Lett. **72**, 2466 (1998)
21 Ü. Özgür, Y.I. Alivov, C. Liu, A. Teke, M.A. Reshchikov, S. Dogan, V. Avrutin, S.-J. Cho, H. Morkoç, J. Appl. Phys. **98**, 041 301 (2005)
22 W.H. Cao, Y.G. Zhao, H.C. Ong, S.T. Ho, J.Y. Dai, J.Y. Wu, R.P.H. Chang, Appl. Phys. Lett. **73**, 3656 (1998)
23 Z.L. Wang, Mater. Today **7**, 24 (2004)
24 T. Dietl, H. Ohno, F. Matsukura, J. Cibert, D. Ferrand, Science **287**, 1019 (2000)
25 T. Fukumura, Y. Yamada, H. Toyosaki, T. Hasegawa, H. Koinuma, M. Kawasaki, Appl. Surf. Sci. **223**, 62 (2004)
26 D.C. Look, B. Claflin, Y.I. Alivov, S.J. Park, Phys. Stat. Solidi A **201**, 2203 (2004)
27 Y. Ohya, T. Niva, T. Ban, Y. Takahashi, Japan. J. Appl. Phys. **40**, 297 (2001)
28 K. Ogata, T. Kawanishi, K. Sakurai, S.-W. Kim, K. Maejima, S. Fujita, S. Fujita, Phys. Stat. Solidi **229**, 915 (2002)
29 H. Kato, M. Sato, K. Miyamoto, T. Yao, J. Cryst. Growth **265**, 375 (2004)
30 T.P. Smith, H. McLean, D.J. Smith, R.F. Davis, J. Cryst. Growth **265**, 390 (2004)
31 S. Zhu, C.H. Su, S.L. Lehoczky, M.T. Harris, M.J. Callahan, P. McCarty, M.A. George, J. Cryst. Growth **219**, 361 (2000)
32 S. Zhu, C.-H. Su, S.L. Lehoczky, M.T. Harris, M.J. Callahan, P. McCarty, M.A. George, J. Cryst. Growth **225**, 190 (2001)
33 F. Hamdani, M. Yeadon, David J. Smith, H. Tang, W. Kim, A. Salvador, A.E. Botchkarev, J.M. Gibson, A.Y. Polyakov, M. Skowronski, H. Morkoc, J. Appl. Phys. **83**, 983 (1998)
34 G. Cantwell, H.P. Xin, Y.B. Yuan, J.J. Song, C.W. Litton, Y.K. Yeo, T. Steiner, ZnO workshop, Sendai, Japan (2004)
35 H. Wenisch, V. Kirchner, S.K. Hong, Y.F. Chen, H.J. Ko, T. Yao, J. Cryst. Growth **227**–**228**, 944 (2001)
36 R. Khanna, K. Ip, Y.W. Heo, D.P. Norton, S.J. Pearton, F. Ren, Appl. Phys. Lett. **85**, 3468 (2004)
37 M.J. Suscavage, D.F. Ryder Jr, P.W. Yip, Mater. Res. Soc. Symp. Proc. **449**, 287 (1997)
38 J. Fryar, E. McGlynn, M. O'Henry, A. Antony Cafolla, C.J. Hanson, Nanotechnology **15**, 1971 (2004)
39 P.R. Willmott, J.R. Huber, Rev. Mod. Phys. **72**, 315 (2000)
40 D.C. Reynolds, C.W. Litton, D.C. Look, J.E. Hoelscher, B. Claflin, T.C. Collins, J. Nause, B. Nemeth, J. Appl. Phys. **95**, 4802 (2004)
41 J. Nause, B. Nemeth, Semicond. Sci. Technol. **20**, 45 (2004)
42 D.B. Eason, G. Cantwell, Ext. Abstr. 2002 International Conference on Solid State Devices and Materials (2002), p. 360
43 S.K. Hong, Y. Chen, H.J. Ko, H. Wenisch, T. Hanada, T. Yao, J. Electron. Mater. **30**, 647 (2001)
44 M.W. Cho, K.W. Koh, K. Morikawa, K. Arai, H.D. Jung, Z. Zhu, T. Yao, Y. Okada, J. Electron. Mater. **26**, 423 (1997)
45 M.J. Callahan, D.F. Bliss, M.T. Harris, N.M. Alexander, in: *Properties, Processes and Applications of ZnO*, ed. by C.W. Litton, D.C. Reynolds, T.C. Collins (IEE IOP, London, 2004), chapt. 8
46 M. Suscavage, M. Harris, D. Bliss, P. Yip, S.Q. Wang, D. Schwall, L. Bouthillette, J. Bailey, M. Callahan, D.C. Look, D.C. Reynolds, R.L. Jones, C.W. Litton, MRS Internet J. Nitride Semicond. Res. **4S1**, G3.40 (1999)
47 J. Nause, B. Nemeth, ZnO workshop, Sendai, Japan (2004)
48 L. Demianets, D. Kostomarov, Ann. Chim. Sci. Mater. **26**, 193 (2001)
49 F.H. Leiter, H.R. Alves, A. Hofstaetter, D.M. Hoffman, B.K. Meyer, Phys. Stat. Solidi B **226**, R4 (2001)
50 N.Y. Garces, L. Wang, L. Bai, L.E. Halliburton, Appl. Phys. Lett. **81**, 622 (2002)
51 Y.M. Strzhemechny, H.L. Mosbacker, D.C. Look, D.C. Reynolds, C.W. Litton, N.Y. Garces, N.C. Giles, L.E. Halliburton, S. Niki, L.J. Brillson, Appl. Phys. Lett. **84**, 2545 (2004)